Nuclear shell model calculations of neutralino-nucleus cross sections for ^{29}Si and ^{73}Ge

M. Ted Ressell,[1,2] Maurice B. Aufderheide,[1,2] Stewart D. Bloom,[1] Kim Griest,[3] Grant J. Mathews,[1,2] and David A. Resler[4]

[1]*P-Division/Physical Sciences Directorate, Lawrence Livermore National Laboratory, Livermore, California 94550*

[2]*Institute of Geophysics and Planetary Physics, Lawrence Livermore National Laboratory, Livermore, California 94550*

[3]*Physics Department, University of California, San Diego, La Jolla, California 92093*

[4]*N-Division/Physical Sciences Directorate, Lawrence Livermore National Laboratory, Livermore, California 94550*

(Received 28 June 1993)

We present the results of detailed nuclear shell model calculations of the spin-dependent elastic cross section for neutralinos scattering from ^{29}Si and ^{73}Ge. The calculations were performed in large model spaces which adequately describe the configuration mixing in these two nuclei. As tests of the computed nuclear wave functions we have calculated several nuclear observables and compared them with the measured values and found good agreement. In the limit of zero momentum transfer we find scattering matrix elements in agreement with previous estimates for ^{29}Si but significantly different than previous work for ^{73}Ge. A modest quenching, in accord with shell model studies of other heavy nuclei, has been included to bring agreement between the measured and calculated values of the magnetic moment for ^{73}Ge. Even with this quenching, the calculated scattering rate is roughly a factor of 2 higher than the best previous estimates; without quenching, the rate is a factor of 4 higher. This implies a higher sensitivity for germanium dark matter detectors. We also investigate the role of finite momentum transfer upon the scattering response for both nuclei and find that this can significantly change the expected rates. We close with a brief discussion of the effects of some of the non-nuclear uncertainties upon the matrix elements.

PACS number(s): 95.30.Cq, 14.80.Ly, 21.60.Cs, 98.62.Gq

I. INTRODUCTION

A host of astronomical evidence points to the existence of large amounts of dark matter in the Universe [1]. Despite the overwhelming amount of evidence for this dark matter's existence, its exact nature remains a mystery. Numerous candidates have been proposed. These include both ordinary baryonic and nonbaryonic matter [2]. Among the best motivated, and hence highly favored, of the nonbaryonic candidates is the lightest supersymmetric particle (LSP). Experimental and theoretical considerations suggest that the LSP is a neutralino $\tilde{\chi}$ made up of a linear combination of the photino, Z-ino, and 2 Higgsinos (or equivalently, the B-ino, neutral W-ino, and 2 Higgsinos):

$$\tilde{\chi}=Z_1\tilde{B}+Z_2\tilde{W}_3+Z_3\tilde{H}_1+Z_4\tilde{H}_2 \ . \tag{1}$$

The neutralino is an ideal dark matter candidate. The motivation for its existence arises naturally in modern theories of particle physics [3], not as an ad hoc solution to the dark matter problem. For a very large region of supersymmetric parameter space, neutralinos provide densities sufficient to account for the mass-energy density of the Universe [4]. The $\tilde{\chi}$ also possesses the virtue of potential detectability. Its detection may be possible in at least two ways: indirectly, through the products of $\tilde{\chi}\tilde{\chi}$ annihilation from capture in the Sun or Earth [5], or directly, via elastic neutralino-nucleus $\tilde{\chi}N$ scattering in a detector [6,7]. In either case, the $\tilde{\chi}N$ elastic scattering cross section is an essential ingredient. In this paper we discuss detailed nuclear structure calculations relevant to $\tilde{\chi}N$ scattering for two important elements: silicon and germanium.

Neutralino-nucleus scattering is governed by physics at several energy scales. The mass and the mixing of the $\tilde{\chi}$, and hence its interactions with quarks, are fixed near the electroweak scale. The spin-dependent interactions of the $\tilde{\chi}$ with protons and neutrons are determined by the distribution of quark spin within the nucleon, which depends upon physics at the QCD scale. There are also spin-independent contributions which depend upon the quark content of the nucleons. At the modest momentum transfers available to dark matter particles ($\sim$1 MeV) the $\tilde{\chi}$ interacts with the entire nucleus, not individual nucleons within it. Thus, nuclear structure plays an important role in determining the strength of the $\tilde{\chi}N$ cross section. The uncertainties inherent in the electroweak and QCD-scale physics can be parametrized in different ways. The electroweak parametrization entails choosing the exact composition and mass of the $\tilde{\chi}$ which, in turn, is determined by parameters in a Lagrangian of a supersymmetric model. At the QCD level there are currently two competing possibilities for the coupling of protons and neutrons to the $\tilde{\chi}$. The currently favored parametrization depends upon the measured quark spin content of the proton determined by the European Muon Collaboration (EMC) [8]. In contrast with these values of the spin content are those derived from the naive quark model (NQM). Experiments are being carried out which will hopefully clarify this issue. In this paper we will investigate the effects of both the EMC and the NQM esti-

mates, as well as the uncertainties in their determination.

At the nuclear level, several attempts have been made to improve the cross-section calculations. Initial investigations into spin-dependent $\tilde{\chi}N$ scattering made use of the independent single particle shell model (ISPSM) in which the character of the nucleus is completely determined by a single unpaired valence nucleon [6,9,10]. Subsequent studies [11–15] have revealed a number of inadequacies of the ISPSM and improved upon its estimates of the scattering matrix element. Engel and Vogel [11] used the odd group model (OGM) and mirror pair β decays, in an extended odd group model (EOGM), to show that the ISPSM can be off by a large factor when nuclei are far from closed shells (see also Ref. [12]). Pacheco and Strottman [13] reached the same conclusion by performing detailed nuclear shell model calculations for several light nuclei. The odd group and shell model treatments obtain good agreement for light nuclei but, as the atomic mass increases, nuclear configuration mixing produces cancellations not considered in the OGM. This is most clearly evident in ^{35}Cl (the largest nucleus considered in Ref. [13]) where the OGM and shell model estimates of the matrix elements differ by roughly a factor of 3 (see Table I). For comparison, in Table I we have also included our calculation of the spin in ^{35}Cl using the same interaction and model space as discussed for ^{29}Si in Sec. II A. It is reassuring to note that the two shell model calculations are in close agreement despite the use of different interactions. This effect has also been seen in ^{93}Nb [14] revealing the need for full shell model calculations of heavier nuclei.

The need for more detailed calculations of the spin content of heavier nuclei is exacerbated by the fact that at least two of the most promising detector programs currently under way are based upon ^{73}Ge and ^{29}Si [15]. Both of these nuclei are likely to have large amounts of configuration mixing, making OGM estimates suspect. Furthermore, both ^{73}Ge and ^{29}Si require very large model spaces. This is why the calculations were not carried out in Ref. [13]. In fact, in a recent review [7] the statement was made that, "...until a reliable calculation in ^{73}Ge has been carried out, the description of the nuclear physics of dark matter detection will be incomplete."

With these last comments as motivation we have used the nuclear shell model code CRUNCHER [16] to perform large basis calculations of ^{73}Ge and ^{29}Si with the aim of providing accurate cross sections for determining event rates for spin-dependent scattering in the Ge and Si detectors currently under development.

All of the work discussed above has been in the zero momentum transfer limit. As the experimental lower limit to the $\tilde{\chi}$ mass continues to increase, finite momentum transfer needs to be considered. This is especially true for heavier nuclei, such as ^{73}Ge [7]. Unfortunately, phenomenological models, such as the OGM and the interacting boson fermion model (IBFM) [17] which have been used in the $q=0$ limit cannot be easily extended to finite momentum transfer. Furthermore, the ISPSM has been shown to be a poor approximation at finite q [7,14,18]. Fortunately, incorporating finite momentum transfer into a full nuclear shell model calculation is straightforward. The formalism is presented in [7]. It is a simple extension of that used in semileptonic weak and electromagnetic interactions with nuclei [19]. In Sec. IV, we show that finite momentum transfer is important for both ^{29}Si and ^{73}Ge.

TABLE I. Summary of the calculated spin of ^{35}Cl.

	$\langle \mathbf{S}_n \rangle$	$\langle \mathbf{S}_p \rangle$
ISPSM	0	−0.3
OGM [7,11]	0	−0.15
EOGM [7,11]	0.014	−0.094
Shell model [13]	−0.011	−0.059
This work	−0.0088	−0.051

II. THE ZERO MOMENTUM TRANSFER LIMIT

Neutralinos in the halo of our Galaxy can be characterized by a mean virial velocity of, $v \simeq \langle v \rangle \simeq 300$ km/sec$=10^{-3}c$. The maximum characteristic momentum transfer in $\tilde{\chi}N$ scattering will be $q_{\max}=2M_r v$ where M_r is the reduced mass of the $\tilde{\chi}N$ system. If the product $q_{\max}R$ is small ($\ll 1$), where R is the nuclear size, the matrix element for spin-dependent $\tilde{\chi}N$ scattering reduces to a very simple form [7,11]

$$\mathcal{M}=A\langle N|a_p\mathbf{S}_p+a_n\mathbf{S}_n|N\rangle\cdot\mathbf{s}_{\tilde{\chi}}\ , \tag{2}$$

where

$$\mathbf{S}_i=\sum_k \mathbf{s}_i(\mathbf{k}),\quad i=p,n \tag{3}$$

is the total nuclear spin operator, k is a sum over all nucleons, and a_p, a_n, are $\tilde{\chi}$-nucleon coupling constants which depend upon the quark spin-distribution within the nucleons and on the composition of the $\tilde{\chi}$, see, e.g., Eqs. (12) and (13) for the specific cases of the $\tilde{B}$ and $\tilde{\gamma}$. Much of the uncertainties arising from electroweak and QCD scale physics are encompassed by a_p and a_n. The normalization A involves the coupling constants, masses of the exchanged bosons and various LSP mixing parameters that have no effect upon the nuclear matrix element. To maintain contact with the previous literature [4,6,10,11,13], we note that Eq. (23) has often been written as

$$\mathcal{M}=A\lambda\langle N|\mathbf{J}|N\rangle\cdot\mathbf{s}_{\tilde{\chi}} \tag{4a}$$

with

$$\lambda=\frac{\langle N|a_p\mathbf{S}_p+a_n\mathbf{S}_n|N\rangle}{\langle N|\mathbf{J}|N\rangle}=\frac{\langle N|(a_p\mathbf{S}_p+a_n\mathbf{S}_n)\cdot\mathbf{J}|N\rangle}{J(J+1)}\ . \tag{4b}$$

Examples of the full $\tilde{\chi}N$ cross section can be found in the Appendix and in Refs. [4,7,10,11]. Calculations of the matrix element in Eq. (2) are straightforward, although computationally intensive, in the nuclear shell model.

Our approach to modeling the nuclei ^{29}Si and ^{73}Ge is quite straightforward in principle. Using a reasonable two-body interaction Hamiltonian we calculate the nu-

clear wave functions in an appropriate model space. As checks on these wave functions we compute the excited state energy level spectrum, the magnetic moments, and the single particle spectroscopic factors for each nucleus and compare them with experimentally measured quantities. Once reasonable agreement between the calculations and measurements is obtained the ground-state wave functions are used to calculate the $\tilde{\chi}N$ nuclear matrix element, $\langle N|a_p\mathbf{S}_p+a_n\mathbf{S}_n|N\rangle$ of Eq. (2). (We present our results using the convention that all angular momentum operators are evaluated in their z projection in the maximal M_J state, e.g., $\langle\mathbf{S}\rangle\equiv\langle N|\mathbf{S}|N\rangle=\langle J,M_J=J|S_z|J,M_J=J\rangle$.) These wave functions are also used to compute the more complicated finite momentum transfer matrix elements. In practice these steps may be quite time consuming. In the following two subsections we detail the steps entailed in calculating the nuclear matrix elements for spin-dependent $\tilde{\chi}N$ scattering with ^{29}Si and ^{73}Ge.

A. ^{29}Si

For the nucleus ^{29}Si, the calculation of the nuclear wave functions and matrix elements is almost as straightforward as presented above, because a well defined and tested interaction in a well-defined model space exists [20]. This greatly facilitates the calculation. In fact, after the completion of these calculations, it was brought to our attention that the calculation of ^{29}Si's spin had already been done, using the same interaction and model space, but in a different context [21]. In spite of this, we will detail our calculation for two reasons. First, the calculation of the ^{29}Si matrix element will serve as a useful comparison for the accuracy of the calculation of ^{73}Ge's matrix element. The ^{29}Si computation will help to establish just how reliably one can use the shell model to determine the relevant observables. Second, we will show in a subsequent section that finite momentum transfers are important for Si and this calculation does not exist in the literature.

For our calculation of the wave functions for ^{29}Si we have used the universal *sd* shell interaction of Wildenthal [20] in a full *sd* shell model space. This interaction has been meticulously developed and tested over many years and is known to accurately reproduce numerous nuclear observables for *sd* shell nuclei. Our computations were performed using the Lanczos method *m*-scheme nuclear shell model code CRUNCHER [16] and its auxiliary codes. The *m*-scheme basis for ^{29}Si in this model space has a dimension of 80115 Slater determinants. The calculation of the wave functions takes roughly a day and a half of time on a dedicated SPARC station.

In Fig. 1 we present the calculated vs the measured energy spectrum [22] for the 10 lowest eigenstates of ^{29}Si. It is clear that good overall agreement is achieved.

A test of more relevance to the $\tilde{\chi}N$ scattering cross section is the comparison between the predicted and measured ground-state magnetic moment for ^{29}Si. This is because of the similarity of the relevant operators. The magnetic moment, μ, is given by

$$\mu=\langle N|g_n^s\mathbf{S}_n+g_n^l\mathbf{L}_n+g_p^s\mathbf{S}_p+g_p^l\mathbf{L}_p|N\rangle\ , \tag{5}$$

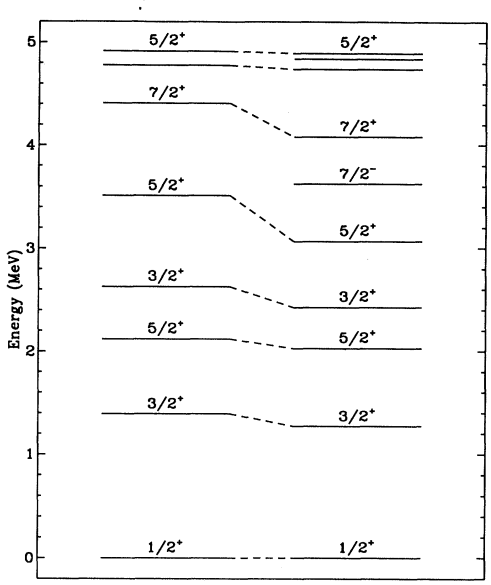

FIG. 1. The calculated (left) and measured [22] (right) excited state energy spectrum of ^{29}Si. The ground state has $J^\pi=\frac{1}{2}^+$. The dashed lines connect states with the same J^π. The J^π values for most of the states have been included for reference.

where the $\mathbf{S}_i$ are the total spin operators (in their z projection) from Eq. (3), and the $\mathbf{L}_i$ are the analogous orbital angular momentum operators. The *free particle* g factors are given by $g_n^s=-3.826$, $g_n^l=0$, $g_p^s=5.586$, and $g_p^l=1$ (in nuclear magnetons). There is ample evidence in shell model calculations for many nuclei that these g factors are quenched. In ^{29}Si this quenching is not necessary and is, in this context, counterproductive. We will address this issue again in a later section (quenching seems to be necessary to get μ "right" in ^{73}Ge). Using our wave functions we find $\mu_{\rm calc}=-0.50$, in agreement with the previous calculation [21]. This is to be compared with the measured value of $\mu_{\rm expt}=-0.555$, which is good agreement by shell model standards. We also note that the ISPSM gives a value of $\mu_{\rm ISPSM}=-1.91$, in strong disagreement with experiment.

As a final check on the accuracy of our wave functions, we have calculated the spectroscopic factors for a number of one nucleon transfer reactions and compared them to the experimentally determined values. Spectroscopic factors $S(J;jJ_0)$ are defined in [23] as

$$S(J;jJ_0)=|\langle\psi(J,M)|\Psi(j,J_0;J,M)\rangle|^2\ , \tag{6}$$

where $\Psi(j,J_0;J,M)$ is the state obtained by coupling an odd nucleon with angular momentum j to the core with angular momentum J_0 to obtain total angular momentum J. $\psi(J,M)$ is the true nuclear wave function. As an example, we compute S for the reaction $^{28}\mathrm{Si}+d\rightarrow{}^{29}\mathrm{Si}+p$ going from the ground state of ^{28}Si, $J=0$, to the total ground state of ^{29}Si, $J=\frac{1}{2}$, in the ISPSM. Since the incoming neutron has spin $\frac{1}{2}$ the only amplitude which can contribute (in the ISPSM) is that in which the neutron is

in a $L=0$ state. Thus, we have $S(\frac{1}{2};\frac{1}{2},0)=1$. [Note, experimental data is generally presented as $(2J+1)S(J;j,J_0)$ and we will adhere to that convention.] In a full shell model calculation (and real nuclei), configuration mixing complicates this simple picture.

To calculate the $S(J;j,J_0)$ for ^{29}Si, we have computed the ground state wave function for ^{28}Si using the same Hamiltonian and model space. As detailed in Ref. [16] we then act on this wave function with a neutron creation operator and take the scalar product of the result with the relevant ^{29}Si wave function. The most important calculation is, of course, the ground state to ground state transition since it most directly probes the nuclear configurations which can interact with the $\tilde{\chi}$. As an additional check, we have calculated the spectroscopic factors to the first two excited states as well. The results of these calculations are presented in Table II along with an unweighted average of the comparable experimental data from Endt [24]. We also present the ISPSM results. Table I reveals the good agreement between the full shell model calculation and experiment as well as the inadequacy of the ISPSM. This provides confidence in our wave functions and our calculations of the $\tilde{\chi}N$ matrix elements.

Once we have suitable wave functions, the nuclear matrix element in Eq. (2) ($\langle N|a_p\mathbf{S}_p+a_n\mathbf{S}_n|N\rangle$) is easily calculated for any set of a_p and a_n. Here we compute the spins in Eq. (2), and then multiply them by the desired a_i to find the total matrix element. In Table III we present the results of this exercise using our wave functions. Our results agree with those found in Ref. [21]. In Table III we also present the results found in the ISPSM, the OGM, and the extended OGM approach. It is immediately apparent that the ISPSM is a very poor approximation to the actual nuclear configuration. Configuration mixing causes the total angular momentum to be shared between the nuclear spin and orbital angular momentum, contrary to the assumptions of the ISPSM (the total angular momentum resides in the spin of the $2s_{1/2}$ neutron). It is also apparent that the OGM treatments and the shell model calculations are in fair agreement as to the properties of ^{29}Si. The important point here is that the protons contribute negligibly to the relevant nuclear properties, the key assumption of the OGM. We will find, however, that this assumption is violated for ^{73}Ge.

B. ^{73}Ge

The availability of a well-developed and tested interaction in the *sd* shell made the calculation of the ^{29}Si ground-state wave function relatively simple. For our calculation of the ground state of ^{73}Ge we did not have the luxury of a good (in the sense that it has been phenomenologically determined and extensively tested) Hamiltonian and there is not a well-defined model space. Hence there is more uncertainty in determining a good nuclear state which accurately reproduces the measured observables. There is some evidence that ^{73}Ge may be deformed [7] meaning that a large model space may be required. The extent to which our wave functions can be trusted will be revealed by how well they reproduce observable phenomena. Our approach has been to choose fairly large model spaces which should include most of the relevant excitations and apply a fairly simple but well-motivated interaction to the nucleons within this space. We then examine the ordering and spacing of the excited state energy levels. The single particle energies (SPE's) of the interaction are then modified and the procedure is repeated. Thus, by a process of iteration, we have been able to reproduce the low-lying energy levels in ^{73}Ge. This procedure has been previously used with some success in this mass region [25]. As before, once a suitable fit to the energy spectrum is obtained, the magnetic moment and spectroscopic factors are calculated as additional checks on the wave function. When we are convinced that we have reasonable wave functions, we then calculate the spin distribution. We now present this procedure in some detail.

In our study of ^{73}Ge, we have chosen to use the Petrovich-McManus-Madsen-Atkinson (PMMA) interaction [26]. This interaction is an analytic approximation to the Kallio and Kolltveit [27] interaction, which is a reasonable approximation to a full G-matrix calculation. This interaction has proven to be both adequate and tractable in shell model calculations. As discussed above, the SPE's were varied in order to match the energy spectrum of low-lying excited states. Using this interaction we have investigated two different model spaces. The first, which we will refer to as the small space, has an m-scheme basis dimension of 24731 Slater determinants. The other, creatively named the large space, allows many more excitations with an m-scheme basis dimension of 117137 Slater determinants. Despite the fairly large size of the bases, rather severe truncations in the space have been enacted. The small space is the smallest in which we could obtain agreement with the spectrum. The large basis dimension was determined by computer time and memory constraints. Each iteration (of which there were many) consumed roughly 4 days of SPARC time and several hundred Mbytes of memory.

TABLE II. Summary of the spectroscopic factors $S(J;jJ_0)$ for ^{29}Si. The experimental values are an unweighted average of the data followed by (in parentheses) the spread in the data, as represented by the low and high measurements, from Ref. [24].

Orbital	J^π	$(2J+1)S_{\text{expt}}$	$(2J+1)S_{\text{calc}}$	$(2J+1)S_{\text{ISPSM}}$
$2s_{1/2}$	$\frac{1}{2}^+$	1.02(0.74−1.5)	0.90	2
$1d_{3/2}$	$\frac{3}{2}^+$	3.62(2.1−5.2)	2.65	4
$1d_{5/2}$	$\frac{5}{2}^+$	1.14(0.53−1.8)	0.85	6

TABLE III. The value of the (z projection) of the nuclear spin and orbital angular momentum matrix elements and the predicted magnetic moments μ (using free particle g factors) for ^{29}Si and ^{73}Ge. The last row contains our values of the large space shell model calculation with an isovector quenching factor of 0.833 applied to the spin matrix elements of the row above. If the magnetic moment has been used as input it is necessarily the measured value and has been enclosed in parentheses.

^{29}Si	$\langle \mathbf{S}_n \rangle$	$\langle \mathbf{S}_p \rangle$	$\langle \mathbf{L}_n \rangle$	$\langle \mathbf{L}_p \rangle$	μ
ISPSM	0.5	0	0	0	−1.91
OGM	0.15	0	0.35	0	(−0.555)
EOGM	0.204	0.054	?	?	(−0.555)
Shell model	0.13	−0.002	0.37	0.019	−0.50
^{73}Ge					
ISPSM	0.5	0	4	0	−1.91
OGM	0.23	0	4.27	0	(−0.879)
IBFM	0.469	−0.009	3.981	0.060	−1.785
IBFM (quenched)	0.245	−0.005	?	?	(−0.879)
Shell model (small)	0.496	0.005	3.596	0.40	−1.468
Shell model (large)	0.468	0.011	3.529	0.491	−1.239
Shell model (large,quenched)	0.372	0.009	3.529	0.491	(−0.879)

Each of these model spaces is "customized" to ^{73}Ge and requires some explanation. In standard notation the small space may be described by $[(1f_{5/2},2p_{3/2},2p_{1/2})^{16}(1g_{9/2})^{1}(2d_{5/2},1g_{7/2})^{0}$ $+(1f_{5/2},2p_{3/2},2p_{1/2})^{16}(1g_{9/2})^{0}(2d_{5/2},1g_{7/2})^{1}$ $+(1f_{5/2},2p_{3/2},2p_{1/2})^{15}(1g_{9/2})^{2}\quad(2d_{5/2},1g_{7/2})^{0}]$. In words, the 16 particles in the $1f_{5/2}$, $2p_{3/2}$, and $2p_{1/2}$ shells may "move" freely about in these shells, there is also 1 particle (a neutron) in the $1g_{9/2}$; additionally, excitations of the $1g_{9/2}$ neutron into the $2d_{5/2}$ or $1g_{7/2}$ shells is allowed, *or* 1 particle from the $1f_{5/2}$, $2p_{3/2}$, and $2p_{1/2}$ shells may be excited into the $1g_{9/2}$ orbital (there it can pair with the already present neutron). In the same notation, the large model space allows configurations given by $((1f_{5/2},2p_{3/2})^{14}(2p_{1/2},1g_{9/2})^{3}(2d_{5/2},1g_{7/2})^{0}$ $+(1f_{5/2},2p_{3/2})^{14}(2p_{1/2},1g_{9/2})^{2}(2d_{5/2},1g_{7/2})^{1}$ $+(1f_{5/2},2p_{3/2})^{13}(2p_{1/2},1g_{9/2})^{4}(2d_{5/2},1g_{7/2})^{0})$. The major difference here is that it is now possible to have up to 4 particles in the $1g_{9/2}$ orbital. In Table IV we list the SPE's used in the small and large space calculations. Comparing these values with the energy level spacings shown in Fig. 2 clearly reveals the effects of the residual PMMA two-body interaction. To further illustrate the rapid increase in the size of the model space, we note that if we extended the large space to include excitations of the type $(1f_{5/2},2p_{3/2})^{14}(2p_{1/2},1g_{9/2})^{1}(2d_{5/2},1g_{7/2})^{2}$ the dimension of the space would be 168597 Slater determinants. A calculation of this size could be done but each iteration to match the energy levels would take an excessive amount of time. Additionally, such configurations are unlikely to play much of a role in the ground-state wave function. The addition to any more excitations would rapidly expand the model space beyond our present capability to calculate the wave functions.

TABLE IV. The relative spacing of the single particle energies (SPE) for the small and large model space calculations of the ^{73}Ge wave functions. The SPE of the $1g_{9/2}$ orbital has been chosen as the zero point for the calculations.

Orbital	SPE (MeV) (small)	SPE (MeV) (large)
$2p_{1/2}$	−1.542	−1.44
$2p_{3/2}$	−1.448	−1.43
$1f_{5/2}$	−3.472	−3.17
$2d_{5/2}$	1.601	1.57
$1g_{7/2}$	−0.718	−1.36
$1g_{9/2}$	0.0	0.0

It is seen from the above, that the calculation of ^{73}Ge's wave functions, ψ, involves active particles in both the fp and the gd shells. This allows for the possibility that our wave functions may contain spurious contributions due to center of mass motion of the nucleus. (There are no cross shell excitations in ^{29}Si, so center of mass excitations are not present.) In a truncated model space such as one is forced to employ in the calculation of ^{73}Ge, there is no accepted way of dealing with these spurious components. In general, they are thought to be small and we now present several lines of reasoning which lead us to believe that the effect of spurious states is small in our calculation. We will discuss only the large space since, as we will show, it provides a more realistic description of the ^{73}Ge wave function. Examining the allowed excitations in ψ discussed above, we see that there are no particle-hole excitations involving the fp and gd shells that involve $\Delta J<2$. This implies that any spurious components will be at least "second order" (i.e., they are at least $2\hbar\omega$ excitations) and highly suppressed. (Possible $\Delta J=2$ transitions that might involve spurious states are between the $1f_{5/2}$ and $1g_{9/2}$ and between the $2p_{1/2}$ and $2d_{5/2}$ shells; all other transitions are more highly suppressed.)

The effects of spurious components of ψ are almost certainly negligible in the calculation of $|\mathcal{M}|^2$, Eq. (2). This is because the spin operator $\mathbf{S}\propto\sigma$, does not mix states in different oscillator shells. Therefore, in calculating $|\mathcal{M}|^2$ the spurious parts will not mix with the nonspurious parts of $\mathcal{M}$ (i.e., if 10% of ψ is spurious, it will only make a 1% contribution to $|\mathcal{M}|^2$). Furthermore, since we are calculating *elastic* scattering, there is no parity change in

the final state and any spurious components are once again of "second order" and expected to be suppressed. Finally, we note that it is possible to examine the make-up of the wave functions by hand and look for contributions from states that could mix with center of mass excitations. While this is impractical for the entire wave function (117137 Slater determinants), we have looked at the most important 100 Slater determinants for the first few eigenstates. For the ground state, these 100 pieces comprise the majority of the wave function $|\psi|^2 \simeq 0.92 \leq 1$, and contain no excitations that can mix with spurious states. Thus, our expectations that spurious states are unimportant are confirmed.

In Fig. 2 we show the excited state energy spectrum of the first 10 calculated states compared to the measured spectrum in the same energy range for both the large and the small spaces. In the small space we were able to iterate until essentially perfect agreement between theory and experiment was obtained for the lowest lying five excited states. There is then a large region where there are many observed states but no calculated states. This is because our limited model space is not large enough to contain all of the 2-particle 1-hole excitations necessary to describe such states. The omission of these seniority 3 configurations, from the ground state, is probably not too serious. At excitation energies $\gtrsim 1$ MeV there are again several calculated states which seem to have analogs in the measured spectrum of states.

With the greater number of available excitations in the large space one would expect to start describing states in the spectrum between 0.5 MeV and 1 MeV, and this is observed for the 10 lowest-lying states, as demonstrated in the right side of Fig. 2. In the large space it was impractical and unnecessary to iterate until "perfect" agreement was obtained for the lowest energy states (compare the scales of Figs. 1 and 2 and the relative errors). We did iterate until the small changes in the SPE's needed to move the states no longer affected the spin matrix elements significantly. Figure 2 reveals reasonable agreement between our low-lying calculated states and the observed distribution of states giving us reasonable assurance that we have obtained a good description of the ^{73}Ge ground state. We now apply our other tests in the hope of confirming this statement.

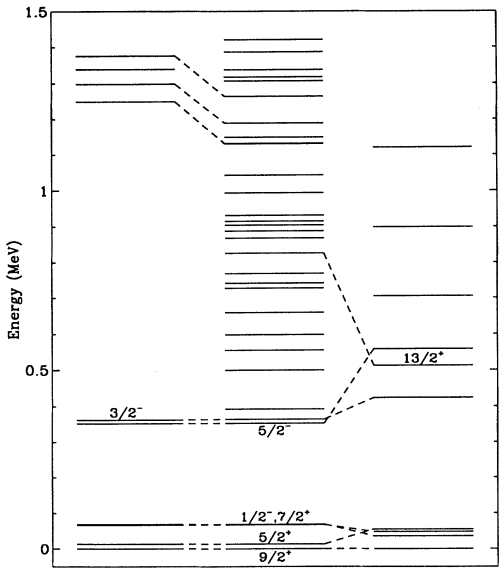

FIG. 2. The calculated small space (left), measured [22] (center), and calculated large space (right) energy spectra of ^{73}Ge. The ground state has $J^\pi = \frac{9}{2}^+$. Where we have felt comfortable with the identifications, we have connected states with identical J^π's by dashed lines. The J^π's for some of the lower-lying states have been noted on the plot.

As previously noted, the most relevant test for the spin matrix elements is the comparison of the magnetic moments. Here our calculations do an acceptable job but some quenching of the g factors is required to obtain complete agreement with experiment. All other attempts to calculate the matrix elements have relied heavily upon quenching as well: the IBFM [17] and the OGM [7,11] (which can be viewed as a well motivated prescription for quenching the ISPSM value of μ). In fact, the quenching required by our wave functions is significantly less than in either of the above methods. We will discuss the issue of quenching in a subsequent section. The measured magnetic moment of ^{73}Ge is $\mu_{\text{expt}} = -0.879$ which is significantly different from the ISPSM value of $\mu_{\text{ISPSM}} = -1.91$. The values we calculate (without quenching) are $\mu_{ss} = -1.468$ for the small space and $\mu_{ls} = -1.239$ for the large space, a major improvement over the ISPSM, especially for the large space. The main reason for the decrease in μ can be seen in Table III. Because of the configuration mixing, the protons significantly contribute to the total angular momentum, especially through their orbital part. Referring to Eq. (5) it is obvious that a large value of $\langle \mathbf{L}_p \rangle$ can have a significant effect on μ. This large value for $\mathbf{L}_p$ is one of the major results of the present work and the primary reason that our answers will differ from those of previous analyses. While one might wish for better agreement between the measured and calculated magnetic moments, by typical shell model standards [28,29], reasonable agreement has been achieved. Thus we continue to have confidence in our results.

The final test we have performed for ^{73}Ge is to compare the calculated and measured spectroscopic factors, Eq. (6), for the reaction $^{72}\text{Ge} + d \rightarrow {}^{73}\text{Ge} + p$ [30]. As with the magnetic moment comparison, we find quite reasonable results, albeit not without some level of ambiguity. We present our results, the experimental data, and the ISPSM values for the three lowest-lying states in Table V. For the ground state to ground-state reaction, labeled $1g_{9/2}$ in Table V, good agreement is obtained between the computed and experimental value for both model spaces. Since this is the reaction which directly tests the state we are interested in, this is quite encouraging. The small space obviously does not allow enough excitations to correctly describe the excited state transitions. The large space does a much better job on the excited states but if one were interested in their properties, a better description might be desirable. Fortunately, we are only interested in the ground state of ^{73}Ge which seem to be adequately described in these model spaces.

TABLE V. Summary of the spectroscopic factors $S(J;jJ_0)$ for ^{73}Ge. The experimental values are an unweighted average of the data followed by (in parentheses) the spread in the data, as represented by the low and high measurements, from Ref. [30].

Orbital				
Large space	J^π	$(2J+1)S_{\text{expt}}$	$(2J+1)S_{\text{calc}}$	$(2J+1)S_{\text{ISPSM}}$
$1g_{9/2}$	$\frac{9}{2}^+$	6.16(5.04–7.35)	3.96	10
$2d_{5/2}$	$\frac{5}{2}^+$	0.29(0.28–0.30)	0.74	6
$2p_{1/2}$	$\frac{1}{2}^-$	0.67(0.52–0.78)	3.3×10^{-4}	2
Small space				
$1g_{9/2}$	$\frac{9}{2}^+$	6.16(5.04–7.35)	5.91	10
$2d_{5/2}$	$\frac{5}{2}^+$	0.29(0.28–0.30)	3.55	6
$2p_{1/2}$	$\frac{1}{2}^-$	0.67(0.52–0.78)	~0	2

After examining the comparisons of the experimental and calculated values of the excited state spectra, magnetic moments, and spectroscopic factors we believe that we have obtained a reasonable description of the ^{73}Ge ground state. The case for this is not unassailable but our wave functions do include pieces of physics which other analyses have neglected and they do reproduce a number of observables with good accuracy. Having established the viability of our calculation of the ground-state wave function of ^{73}Ge, we now discuss ^{73}Ge-$\tilde{\chi}$ scattering.

The primary results of this section have already been presented in Table III, which shows our results for the spin and orbital pieces of total angular momentum (in their z projection). We compare our results to those found in the ISPSM, the OGM, and the IBFM. We will confine our comments henceforth to the large space calculation since it seems to be a better representation of the ground state. The small space serves primarily to illustrate the sensitivity to configuration mixing. The fact that an increase in the size of the model space leads to an improvement in the magnetic moment is especially heartening. Table III shows that these effects are small but finite. As a final comment regarding Table III before we discuss its contents, we point out that: there are two rows for the IBFM, in the first row the required quenching should be applied to a_p and a_n in the matrix elements (this corresponds to quenching the g factors for μ), in the second the same quenching has, instead, been applied to the spins [7] (here the free particle g factors would be used for the magnetic moment). These two approaches are equivalent but help to highlight the different results obtained in the IBFM and shell model approaches.

The most interesting feature of Table III is the large contribution of the proton's orbital angular momentum found in our calculations. This large value of $\langle \mathbf{L}_p \rangle$ results in significant difference in the spin matrix elements found in this investigation vs those found in the OGM and IBFM approaches. The proton's orbital angular momentum makes a major contribution to the magnetic moment which is completely neglected in the OGM and not adequately represented in the IBFM. Surprisingly (and coincidentally), our results for the spin tend to agree with those found in the ISPSM. A large contribution to the angular momentum by the protons violates the assumptions of the OGM. This explains the factor of 2 difference in $\langle \mathbf{S}_n \rangle$ between the OGM and our approach. In a shell model treatment of ^{93}Nb, a similar result was found [14], except there the neutrons carry a large amount of orbital angular momentum. In both of these cases the seemingly large violation of the OGM assumptions arises because of the large ground state angular momenta of the nuclei. Both ^{73}Ge and ^{93}Nb are $\langle \mathbf{J} \rangle = 9/2$ nuclei, which implies an angular orbital momentum value of $\langle \mathbf{L} \rangle \simeq 4$. Thus even a small violation of the OGM's assumption that the even group carries no angular momentum can lead to a significant value of $\langle \mathbf{L}_{\text{even}} \rangle$. To make this more concrete consider our results for ^{73}Ge. Here, $\langle \mathbf{L}_p \rangle / \langle \mathbf{J} \rangle \simeq 10\%$ so the protons carry only a small amount of the total angular momentum. However, because of the large value of $\langle \mathbf{J} \rangle$, we find that $\langle \mathbf{L}_p \rangle$ and $\langle \mathbf{S}_n \rangle$ are roughly equal in magnitude; leading to the discrepancy between the shell model results and those of the OGM. The IBFM wave functions do not possess a large proton contribution to the angular momentum of the nucleus and hence produce an unquenched magnetic moment of $\mu_{\text{IBFM}} = -1.785$, similar to the single particle model. This is to be contrasted with the shell model value of $\mu = -1.239$. Thus, in the IBFM a very large quenching factor of 0.523 must be applied to the spin matrix elements (i.e., either a_i *or* $\langle \mathbf{S}_i \rangle$ as is shown in Table III) in order to match the measured magnetic moment of $\mu_{\text{expt}} = -0.879$. If the same procedure is applied to the shell model matrix elements (a procedure we do not recommend, see the next section) a quenching factor of only 0.792 is required. This is considerably less quenching of the spin than in the IBFM. If we apply this quenching factor to the large space spins in Table III (in the same manner as was done to create the second IBFM row), we find $\langle \mathbf{S}_n \rangle = 0.371$ and $\langle \mathbf{S}_p \rangle = 0.009$, still quite different from the OGM and the IBFM (and now the ISPSM) results. Thus, we find that a full shell model calculation using realistic wave functions obtains significantly different values for the spin matrix elements than previous analyses. In fact, our results could result in up to a *fourfold* increase in the $\tilde{\chi}N$ scattering rate over the estimates in previous work. This implies a much greater sensitivity for germanium dark matter detectors. We are now ready to investigate the scattering response at finite momentum

transfer but first we address the issue of quenching in more detail.

III. QUENCHING OF THE SPIN MATRIX ELEMENTS

The concept of quenching of the magnetic moment g factors and Gamow-Teller strength function in shell model calculations has a long history. What is clear is that quenching is almost universally required once nuclei are filled beyond the p shell. To quote from a thorough investigation of the $M1$ (magnetic moment) operator in the *sd* model space [28], "There are several reasons why even 'perfect' shell-model calculations of electromagnetic matrix elements based on the free-nucleon characteristics of the neutron and proton should differ from the corresponding experimental values. In reality, the nuclear wave functions must be more complicated than those of the theoretical model we use. Real nuclear states must involve nucleonic degress of freedom beyond the *sd*-shell space. In addition, non-nucleonic degrees of freedom which involve Δ isobars and mesons may be important in the observed phenomena." This "excluded" physics also plays a role in weak interaction calculations [31]. The preferred method for dealing with these inadequacies of the shell model is to quench the relevant g factors and so construct an effective magnetic moment operator. In the *sd* [28] and *fp* [29] shells, systematic studies have been made to determine the values of modified g-factors which give the best fit to the magnetic moment for a large number of nuclei in each shell. In the *sd* shell study, the operator $(\mathcal{Y}^{(2)}\otimes\mathbf{s})^{(1)}$ was shown to make a significant contribution to the effective magnetic moment operator making comparisons between μ and $\tilde{\chi}N$ matrix element somewhat more ambiguous. We can use these optimized g factors to estimate the amount of quenching we expect for our calculations of $\tilde{\chi}N$ scattering on ^{29}Si and ^{73}Ge.

As mentioned above, quenching in the *sd* shell with the USD interaction has been thoroughly investigated and an optimum set of quenched g factors has been found [28]. Following Table III of [28] the optimized g factors for ^{29}Si should be $g_n^s=-3.24$, $g_p^s=4.75$, $g_n^l=-0.091$, and $g_p^l=1.129$. We note that these spin g values are consistent with an overall spin quenching factor of ~ 0.85. However, we see that it is not only the spin g factors which are modified. Using these values of the g factors in Eq. (5) leads to the following magnetic moment μ(quenched)$=-0.45$, slightly worse than obtained with no quenching. This is not surprising, since the above values of the q's were obtained as a global fit to many *sd*-shell nuclei other than ^{29}Si. Since the wave function for ^{29}Si already matches the measured magnetic moment it is not surprising that quenching damages the agreement. In view of this we do not advocate any quenching for the ^{29}Si matrix elements.

As with all other aspects of this investigation, things become considerably more complicated when we consider ^{73}Ge. Because of the complexity of the nuclei in this mass region, no systematic studies of quenching have been done. The nearest relevant study of which we are aware involves nuclei in the lower *fp* shell with $41\leq A\leq 49$ [29]. In this work, three different interactions are compared and three very different results emerge for the quenched g factors. Additionally, all three estimates of the optimized g factors result in improved agreement between the measured and calculated magnetic moment of ^{73}Ge. For purposes of comparison, in Table VI we show the free particle g factors, the 3 sets of quenched g factors from Ref. [29], and the resultant magnetic moment of ^{73}Ge obtained using the large space wave function. The key point of Table VI is that changes in one of the g's can be compensated for by changes in another and the choice of the best set is dependent upon the interaction chosen. Table VI reveals that the effective g factors from the Kuo-Brown 1 (KB1) [29] interaction produce the best fit to μ_{expt} for ^{73}Ge. These g factors result from an almost exclusive quenching of the *isovector* part of the spin (isovector quenching factor $=0.86$).

There is one additional piece of information which may be used to investigate the required quenching, namely, Gamow-Teller (GT) β decays. As with the magnetic moment operator, the GT operator ($\propto g_A\tau_{\pm}\mathbf{S}$) requires quenching when comparing shell model GT strengths to the measured values [31]. Since the GT operator is directly related to the isovector part of the spin, it is a further probe of the quenching of the isovector spin. Several studies have shown that the free nucleon value of $g_A=1.25$ is *on average* reduced to a value of $g_A\simeq 1$ in heavy nuclei. This corresponds to an isovector spin quenching factor of 0.8. This is in reasonable accord with the isovector quenching of the KB1 interaction discussed above and the similar quenching factor found in the *sd* shell near $A=28$, $(4.00/4.76=0.84)$ [28]. Finally, we note that this GT quenching plays a role in the mirror pair analysis of Engel and Vogel (through their ratio R) [11]. The issue of quenching is thus quite general and quite troublesome when dealing with spin matrix elements of heavy nuclei.

The calculated magnetic moment for ^{73}Ge with free particle g factors already shows significant improvement in agreement with measured values over previous treatments due simply to the inclusion of configuration mixing. If *exact* agreement is desired, an effective operator, with quenched g factors must be invoked. If quenching is invoked, we advocate quenching only the isovector spin part. Following this prescription a quenching of the isovector spin g factor by a factor of 0.833 produces a calculated magnetic moment (large space) of $\mu=-0.879$, in perfect agreement with experiment. This quenching factor is in agreement with the expectations of GT decay in heavy nuclei. In addition, it is consistent with the isovec-

TABLE VI. The sets of quenched g factors used in Ref. [29] and their effect upon the magnetic moment of ^{73}Ge using the large space wave functions.

Interaction	g_n^s	g_p^s	g_n^l	g_p^l	μ
Free	−3.826	5.586	0	1	−1.239
FPD6	−3.41	6.75	0.05	0.71	−0.995
FPMI3	−2.53	5.87	−0.11	0.87	−1.079
KB1	−3.19	4.87	0	1	−0.948
Experiment					−0.879

tor quenching found in the *sd* [28] and *fp* [29] shells when fitting to magnetic moment data. By following this prescription we follow the path with greatest motivation and obtain agreement with experiment by quenching only one number, the isovector component of the spin. Using this quenching factor we find effective spin g factors of $g_n^s(\text{eff}) = -3.04 = 0.795 g_n^s(\text{free})$ and $g_p^2(\text{eff}) = 4.80 = 0.859 g_p^s(\text{free})$. In the zero momentum transfer limit this quenching is equivalent to the large space matrix elements becoming $\langle \mathbf{S}_n \rangle = 0.372$ and $\langle \mathbf{S}_p \rangle = 0.009$ (when combined with the free particle g-factors). These values should be viewed as lower limits to the spin-matrix elements. These values remain quite different from any of the previous estimates performed in the ISPSM, OGM, or IBFM.

We have discussed the quenching of both the GT and the μ operators to illustrate how ubiquitous this phenomena is in shell model calculations. It is, however, worth noting that the quenching of these two operators arises in slightly different manners. Both the GT and the isovector spin part of μ have a similar structure, $\propto \sigma\tau$, and are equally quenched by core polarization effects and the excitation of the Δ isobar [28]. Because the operator μ derives from a vector current, meson exchange currents (MEC's) can also play an important role in quenching the magnetic moment. The GT operator results from axial-vector currents (in particular, the multipoles $\mathcal{T}_L^{el5}$ and $\mathcal{L}_L^5$, discussed in the next section) and the effects of MEC's are highly suppressed for this operator. Similarly, since the $\tilde{\chi}N$ scattering operator, Eq. (2), comes from an axial-vector current, we expect that MEC's will not play a role in the quenching of a_n and a_p. Core polarization, Δ excitation, and MEC's also play a role in quenching the other isovector magnetic moment g factors. MEC effects are dominated by the isovector pions and therefore do not play a significant role in the quenching of the isoscalar pieces of μ.

Because there are a number of different effects which combine to produce the quenching for a specific operator in a specific nucleus, it is extremely difficult to determine what the correct scheme ought to be for $\tilde{\chi}N$ scattering. This is why we have opted for the simplest scheme which is consistent with previous empirical studies and theoretical expectations [28]. By quenching only the isovector spin part of the operator by an amount consistent with previous studies of the GT and μ operators, we find a simple and reasonable prescription for quenching the $\tilde{\chi}N$ scattering matrix element. It does bear remembering that the various competing effects could shift the correct quenching factor around, at about the 10% level, but almost certainly not enough to bring consistency with the OGM predictions.

In this section we have shown that a simple quenching of the isovector-spin matrix element by a factor of 0.833 produces agreement with the measured magnetic moment data for ^{73}Ge. A quenching factor of this type, and roughly this magnitude, could have been predicted based upon previous shell model studies [28,29,31]. Given the amount of evidence which supports this quenching, we feel that the quenched values for the spin matrix elements are the ones most likely to be correct. Hence in calculating the ^{73}Ge-$\tilde{\chi}$ scattering cross section, one should use the values in the last row of Table III (labeled "large, quenched") and the normal a_n and a_p *or* use the values in the row above that with a quenching factor of 0.833 applied to the isovector combination of a_n and a_p while the isoscalar combination remains unchanged. [To be more explicit, calculate $a_1 = a_p - a_n$ and $a_0 = a_p + a_n$ where nothing has yet been quenched. Using these values of a_0 and a_1 recalculate a_p and a_n but now quench the isovector piece, $a_p = \frac{1}{2}(a_0 + 0.833 a_1)$ and $a_n = \frac{1}{2}(a_0 - 0.833 a_1)$. These quenched values of the a_i's may now be combined with the values of the spin in second to last line of Table III to calculate the total matrix element.] Having addressed the issue of quenching, we may now consider $\tilde{\chi}$ scattering with ^{29}Si and ^{73}Ge at finite momentum transfer. For simplicity, at finite momentum transfer, any quenching will be applied to a_n and a_p, as described in the square brackets above or in the appendix, and not to the spin matrix elements. We say a bit more about this in the next section.

IV. FINITE MOMENTUM TRANSFERS

When the LSP was first proposed as a viable dark matter candidate, its preferred mass was between 5 and 10 GeV [32]. With a mass of this order and a typical galactic halo velocity ($v \simeq 10^{-3}c$), the neutralino's total momentum ($q \sim M_r v \sim 10$ MeV) was small compared to the inverse of the nuclear size ($1/R \sim 1/1$ fm ~ 200 MeV) and the zero momentum transfer limit was appropriate for studies of $\tilde{\chi}N$ scattering. Since then, experiments at accelerators have pushed the allowed $\tilde{\chi}$ mass, $m_{\tilde{\chi}}$, to larger values (there are ways around this if some of the theoretical assumptions are relaxed [33]), and it has been shown that heavy $\tilde{\chi}$'s are just as viable as a dark matter candidate as the lighter ones [4,34]. As $m_{\tilde{\chi}}$ becomes larger than a few 10's of GeV the product qR starts to become non-negligible and finite momentum transfer *must* be considered for heavier nuclei. (The maximum allowed momentum transfer is $q_{\max} = 2M_r v$.) In Ref. [7] a simple set of rules is given for when finite momentum transfers are *not* important: i.e., the product $q_{\max} R < 1$ if (a) $A < 28$ or (b) $m_{\tilde{\chi}} < [1/(1.2A^{4/3} + 100)]$ GeV. Thus, we see that finite momentum transfers may be important in ^{29}Si and are quite likely to be important for ^{73}Ge. In this section we will show that these effects are important for both ^{29}Si and ^{73}Ge. For spin-independent scattering these effects have been considered in Refs. [9,4]. For spin-dependent scattering a simple approximation for finite momentum transfer was applied in [12].

The formalism for elastic $\tilde{\chi}N$ scattering at all momentum transfers has been developed in Refs. [7,18]. It is a straightforward extension of the formalism developed for the study of weak and electromagnetic semileptonic interactions in nuclei [19]. The differential $\tilde{\chi}N$ cross section is given by

$$\frac{d\sigma}{dq^2} = \frac{8G_F^2}{(2J+1)v^2} S(q) , \tag{7}$$

where $S(q)$ is the spin structure function

$$S(q)=\sum_{L\ \text{odd}}(|\langle N\|\mathcal{T}^{el5}_L(q)\|N\rangle|^2+|\langle N\|\mathcal{L}^5_L(q)\|N\rangle|^2)\ . \tag{8}$$

$\mathcal{T}^{el5}(q)$ and $\mathcal{L}^5(q)$ are the transverse electric and longitudinal multipole projections of the axial vector current operator [19]. For their explicit form in the $\tilde{\chi}$ context, see [7,18]. The reduced matrix elements of the multipoles in Eq. (8) are easily evaluated in the harmonic oscillator basis in the nuclear shell model [19]. In the limit of zero momentum transfer $S(q)$ reduces to [7,18]

$$S(0)=\frac{1}{4\pi}|\langle N\|\sum_i\frac{1}{2}(a_0+a_1\tau_3^i)\sigma_i\|N\rangle|^2 \tag{9a}$$

or, equivalently,

$$S(0)=\frac{1}{4\pi}|(a_0+a_1)\langle N\|\mathbf{S}_p\|N\rangle +(a_0-a_1)\langle N\|\mathbf{S}_n\|N\rangle|^2\ , \tag{9b}$$

where a_0 (a_1) is the isoscalar (isovector) projection of the a_n and a_p of Eq. (2) ($a_0=a_n+a_p$ and $a_1=a_p-a_n$). To make the connection with the zero momentum transfer case even clearer, we can "unreduce" the matrix elements in Eq. (9b) and rewrite it as

$$S(0)=\frac{1}{\pi}f(N)|a_p\langle N|\mathbf{S}_p|N\rangle+a_n\langle N|\mathbf{S}_n|N\rangle|^2\ , \tag{9c}$$

where the matrix elements in Eq. (9c) now correspond to the entries in Table III. The factor $f(N)$ accounts for the Wigner 3-J function which relates the reduced and unreduced values of the matrix elements and has the values $f(^{29}\text{Si})=6$ and $f(^{73}\text{Ge})=12.222$. Thus, Eq. (8) reduces to the correct expression in this limit. As an aid in discussing the most general neutralino state, $S(q)$ may be split into a pure isoscalar piece S_{00}, a pure isovector piece S_{11}, and an interference term S_{01}, in the following way:

$$S(q)=a_0^2S_{00}(q)+a_1^2S_{11}(q)+a_0a_1S_{01}(q)\ . \tag{10}$$

Two factors contribute to the maximum allowed momentum transfer. As $m_{\tilde{\chi}}$ becomes much greater than the nuclear mass, m_N, the reduced mass asymptotes to $M_r\rightarrow m_N$. Also, the $\tilde{\chi}$'s have a Maxwellian velocity distribution in the halo and some will possess velocities significantly greater than $\langle v\rangle\simeq10^{-3}c$. A maximum velocity of $v_{\max}\simeq2\langle v\rangle$ implies maximum momentum transfers of $q_{\max}(^{29}\text{Si})\simeq108$ MeV and $q_{\max}(^{73}\text{Ge})\simeq271$ MeV. Neither of these values is *small* compared to the inverse nuclear size. In a harmonic oscillator basis, the fiducial nuclear size is set by the oscillator parameter, $b=1$ fm $A^{1/6}=(1/197.327\ \text{MeV})\text{A}^{1/6}$ [23]. Hence we have values $b(^{29}\text{Si})\simeq1.75$ fm and $b(^{73}\text{Ge})\simeq2.04$ fm. These values result in the products $(q_{\max}b)_{\text{Si}}=0.96$ and $(q_{\max}b)_{\text{Ge}}=2.80$. The effects of nonzero momentum transfer might play an important role in these nuclei (depending upon the $\tilde{\chi}$ mass). The nuclear multipole matrix elements in Eq. (8) are most easily evaluated and discussed in terms of the quantity $y\equiv(bq/2)^2$. We will use both y and q in our discussion. The corresponding maximum values of y are $y_{\max}(^{29}\text{Si})=0.23$ and $y_{\max}(^{73}\text{Ge})=1.96$.

Having determined the relevant range of momentum transfers to investigate, we may now discuss the results obtained for the spin structure function, $S(q)$ of Eqs. (8)–(10), using our wave functions for ^{29}Si and the large space wave functions for ^{73}Ge. In Figs. 3 and 4 we display the functions $S_{00}(y)$, $S_{11}(y)$, and $S_{01}(y)$ for ^{29}Si and ^{73}Ge, respectively. With these functions it is a simple matter to calculate $S(q)$ for any $\tilde{\chi}$ once the relevant a_0 and a_1 are known. As an aid in this endeavor we have made simple exponential fits to $S(q)$ for both ^{29}Si and ^{73}Ge. We find that, for ^{29}Si,

$$S^{\text{fit}}_{\text{Si}}(y)=0.00818(a_0^2e^{-4.428y}+1.06a_1^2e^{-6.264y} -2.06a_0a_1e^{-5.413y}) \tag{11a}$$

provides a highly accurate fit to $S(y)$ for $y<0.15$. Beyond this value of y Eq. (11a) begins to seriously underestimate the value of $S(y)$. The equivalent function for ^{73}Ge is

$$S^{\text{fit}}_{\text{Ge}}(y)=0.20313(1.102a_0^2e^{-7.468y} +a_1^2e^{-8.856y}-2.099a_0a_1e^{-8.191y})\ , \tag{11b}$$

valid for $y<0.2$. These two fits should give reasonable values for $S(q)$ in their region of validity for most neutralinos. We note that, if we assume $q=M_rv$, $y=0.1$ corresponds to $m_{\tilde{\chi}}\simeq600$ GeV for ^{73}Ge, already at the upper end of interesting $\tilde{\chi}$ masses. Thus, Eqs. (11) lack of validity at high $y(q)$ should not be a serious impediment to their use. A more serious problem with the fits in Eq. (11) occurs when $a_p\gg a_n$ (or equivalently, when $a_0\simeq a_1$). In this regime of $\tilde{\chi}$ parameter space, there is a near cancellation of S_{00} and S_{11} against S_{01} and the fits do not accurately reproduce the full result. This is a problem for the NQM values of a_n and a_p for a pure $\tilde{B}$, for example (these are given below). For a true representation of $S(q)$ in this case, one must use the full shell model results as presented in Figs. 3 and 4 for all y. With that warning, the fits in Eq. (11) should be quite useful for determining

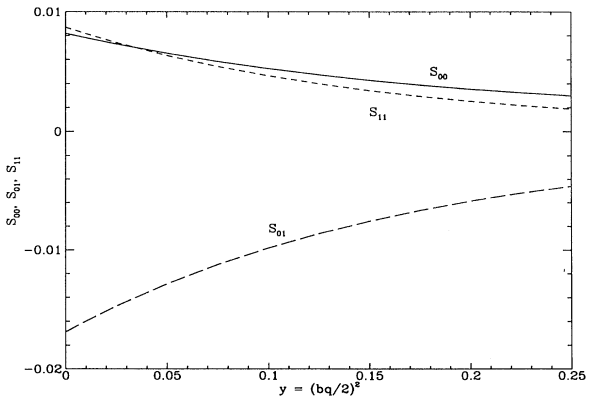

FIG. 3. The calculated functions S_{00}, S_{01}, and S_{01} from Eq. (10) for ^{29}Si as a function of y. The solid line $=S_{00}$, the short dashed line $=S_{11}$, and the long dashed line $=S_{01}$.

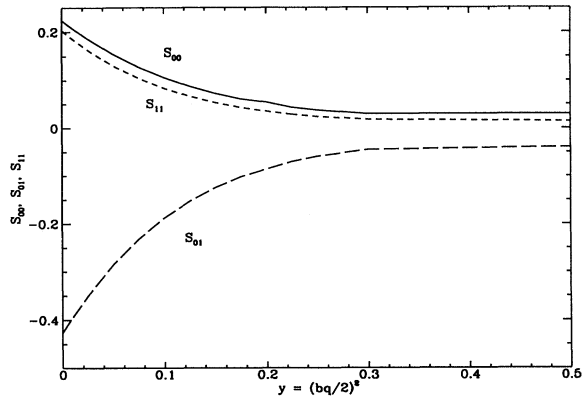

FIG. 4. The calculated functions S_{00}, S_{11}, and S_{01} from Eq. (10) for ^{73}Ge (large space) as a function of y. The solid line $=S_{00}$, the short dashed line $=S_{11}$, and the long dashed line $=S_{01}$.

$S(q)$ for the great majority of $\tilde{\chi}$ cases. Quenching is implemented in Eqs. (11) by making the substitution $a_1 \rightarrow 0.833 a_1$.

In Figs. 5 and 6 we display $S(q)$ for a pure $\tilde{B}$ ($Z_1=1$, $Z_2=Z_3=Z_4=0$). Theoretical arguments lead one to believe that an almost pure $\tilde{B}$ (purity $>99\%$) is the most favored $\tilde{\chi}$ composition once $m_{\tilde{\chi}}$ becomes large enough that finite momentum effects become important [34,35]. (The symmetric or antisymmetric linear combinations of $\tilde{H}_1$ and $\tilde{H}_2$ are also favored configurations.) For a pure $\tilde{B}$ the $\tilde{\chi}$-nucleon couplings are determined by [4]

$$a_{p(n)} = \left\{ \frac{1}{2\cos^2\theta_W} \sum_{u,d,s} \Delta q [(T_{3L} - e_q)^2 + e_q^2] \right\} \zeta_q \ , \qquad (12)$$

$$\zeta_q = -2 \frac{m_W^2}{m_{\tilde{q}}^2 - m_{\tilde{\chi}}^2} \sin^2\theta_W \ ,$$

where θ_W is the weak angle, T_{3L} is the third component of weak isospin, e_q is the charge of the quark, and Δq is the fraction of the nucleon's spin carried by each flavor of quark (see the Appendix). The sum is over the up, down, and strange quarks in the nucleon. The term in the curly brackets has often been referred to as $a_{p(n)}$ in much of the previous literature [10,11,13]. Following Ref. [36] the EMC values for the proton Δq's are $\Delta u = 0.78$, $\Delta d = -0.50$, and $\Delta s = -0.16$, all with an uncertainty of ± 0.08. Inserting these values into Eq. (12) gives $a_p = 0.179\zeta_q$ and $a_n = -0.097\zeta_q$, or equivalently, $a_0 = 0.082\zeta_q$ and $a_1 = 0.276\zeta_q$. The NQM values of the spin content are [37] $\Delta u = 0.93$, $\Delta d = -0.33$, and $\Delta s = 0.0$ resulting in $a_p = 0.254\zeta_q$ and $a_n = -0.017\zeta_q$ ($a_0 = 0.237\zeta_q$, $a_1 = 0.271\zeta_q$).

In Fig. 5 we show $S(q)$ for ^{29}Si using the shell model calculations discussed in Sec. II A. The solid line is computed using the EMC values of $a_{p(n)}$ and the dashed line results from using the NQM values. For ^{29}Si, the response is dominated by the contribution from neutrons. Hence, the small value of a_n in the NQM leads to a severe depression in the calculated matrix element. In Fig. 6(a) we plot $S(q)$ for ^{73}Ge using the same set of a's. Here we see similar behavior but with a much larger amplitude due to the larger amount of spin carried by the

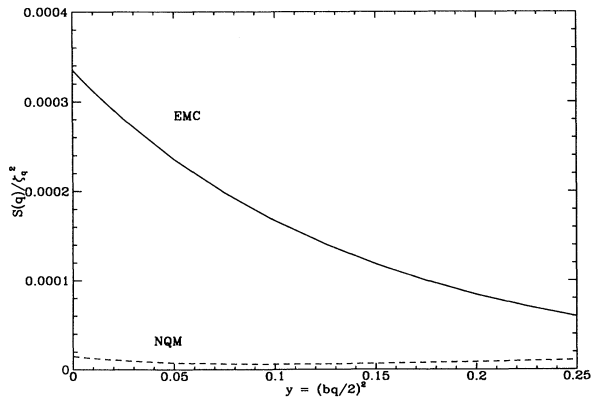

FIG. 5. The spin structure function $S(q)$ for a pure $\tilde{B}$ scattering with ^{29}Si. The solid line is derived using the EMC values for $a_{n(p)}$; the dashed line uses the NQM estimates of these couplings.

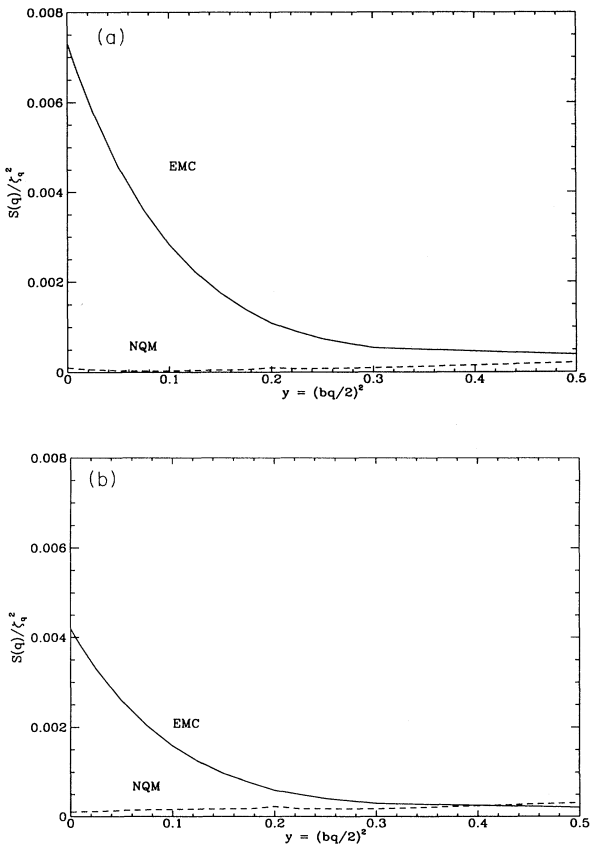

FIG. 6. (a) The spin structure function $S(q)$ for a pure $\tilde{B}$ scattering with ^{73}Ge (large space). The solid line is derived using the EMC values for $a_{n(p)}$; the dashed line uses the NQM estimates for these couplings. (b) The same as (a) but with an isovector quenching factor of 0.833 applied to enforce agreement with the measured magnetic moment at $q=0$ ($a_1 \rightarrow 0.833 a_1$).

neutrons in ^{73}Ge $\{[\langle \mathbf{S}_n \rangle_{\mathrm{Ge}}/\langle \mathbf{S}_n \rangle_{\mathrm{Si}})^2 = (0.47/0.13)^2 \simeq 13\}$. Clearly ^{73}Ge is a better choice as a detector for the pure $\tilde{B}$ case. Next, in Fig. 6(b) we present $S(q)$ for ^{73}Ge where we have quenched the isovector coupling constant in accordance with the discussion of Sec. III, $a_1' = 0.833 a_1 = 0.230 \zeta_q$ for the EMC result. The quenching results in an overall decrease in the amplitude of $S(q)$ for the EMC cross section and a slight increase in the NQM counterpart.

For completeness, we mention one last caveat regarding the above prescription for quenching a_n and a_p for all values of y. It is possible [18], that only the lowest ($L=1$) multipole components in Eq. (8) are quenched, while the higher multipoles may be unquenched (or quenched to a lesser degree). For ^{29}Si this is irrelevant since quenching is not required for this nucleus and only the $L=1$ multipoles contribute. For ^{73}Ge this alternate prescription would change the shape of $S(q)$ very slightly. At small values of y (or equivalently q), $S(q)$ will be completely dominated by the $L=1$ multipoles and the quenched curve for $S(q)$ will be that presented, e.g., in Fig. 6(b) for a pure $\tilde{B}$. At larger values of y ($y \gtrsim 1$) the $L>1$ multipoles will begin to dominate $S(q)$ and the curves in Fig. 6(a) would become more appropriate for a pure $\tilde{B}$. At $y=0.5$, the $L=1$ multipole is still dominant but the higher multipoles are starting to become important. Hence, for a pure $\tilde{B}$, the curve would lie somewhere between the two curves in Figs. 6(a) and 6(b). Similar statements hold for more general $\tilde{\chi}$ states. Given the rather small effect that this alternate quenching scheme has, as well as the fact that it may be no better motivated than the simpler method, we maintain that the simple quenching of a_n and a_p (a_1), for all multipoles equally, described here remains a reasonable prescription.

Finally, in Fig. 7 we present $S(q)$ for a photino scattering with ^{73}Ge. A photino massive enough to make finite momentum effects relevant is highly unlikely [34,35]. However, Fig. 7 is useful, both because a pure photino has often been considered in the literature, and because it illustrates the effects upon $S(q)$ of changing a_n and a_p.

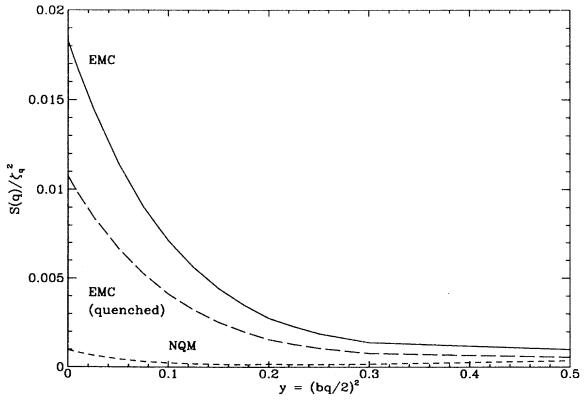

FIG. 7. The spin structure function $S(q)$ for a pure $\tilde{\gamma}$ scattering with ^{73}Ge (large space calculation). The solid line uses the EMC values for $a_{n(p)}$, the long dashed line uses these values but with the isovector piece quenched by a factor of 0.833, and the short dashed line uses the NQM estimates for $a_{n(p)}$.

For a pure photino, the nucleon couplings are

$$a_{p(n)} = \left\{ \sum_{u,d,s} \Delta q e_q^2 \right\} \zeta_q \ , \tag{13}$$

resulting in $a_p = 0.273 \zeta_q$ and $a_n = -0.153 \zeta_q$ for the EMC values of the spin content and $a_p = 0.376 \zeta_q$ and $a_n = -0.043 \zeta_q$ for the NQM estimates. Now that we have presented our results, we may compare them to other work.

In Fig. 8 we compare $S(q)$ for our ^{29}Si result with the shell model (solid line), the single particle model (dashed line), and the single particle model quenched so that $S(0)$ agrees with the OGM prediction (dash-dotted line). This last is not self-consistent but it is the only way to extend the OGM to finite momentum transfers [12]. Two things are immediately apparent from Fig. 8. First, the unquenched ISPSM grossly overpredicts the value of $S(q)$ for all q. Second, the ISPSM with OGM quenching seems to do a very good job of predicting $S(q)$. We quench by reducing a_n by the factor $0.15/0.50 = 0.3$. There is a slight difference in their $q=0$ normalization that is maintained throughout (see Table I). This mismatch would be exacerbated by using the value of $\langle \mathbf{S}_n \rangle \simeq 0.2$ of the EOGM [7,11]. There is also a very slight difference between the shapes of the ISPSM and the shell model results but this appears rather trivial.

Figure 9 is the ^{73}Ge counterpart to Fig. 8. Here, $S(q)$ is plotted for the large space shell model results with no quenching (solid line); the large space shell model result with an isovector quenching factor of 0.833 (long dashed line); the ISPSM with and without a similar isovector quenching (dotted and short dashed lines, respectively); and the ISPSM quenched to agree with the OGM at $q=0$ (dot-dashed line). The most relevant comparison is between the shell model results, quenched or unquenched, and the ISPSM results quenched to agree with the OGM at $q=0$ [$a_n \rightarrow (0.23/0.5) a_n$]. We see that there is a very large discrepancy of either a factor ~ 2 or ~ 4 for the $\tilde{B}$

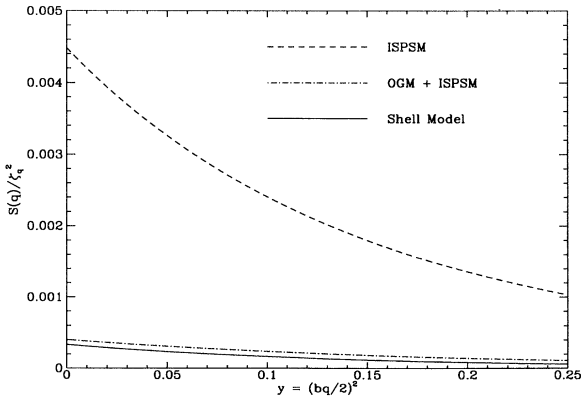

FIG. 8. The spin structure function $S(q)$ for a pure $\tilde{B}$ (EMC couplings) scattering with ^{29}Si for three different models. The solid line is the shell model result and corresponds to the solid line in Fig. 5. The dashed line is the ISPSM result. The dot-dashed line is the ISPSM structure function with a_n quenched so that $S(0)$ agrees with the OGM result.

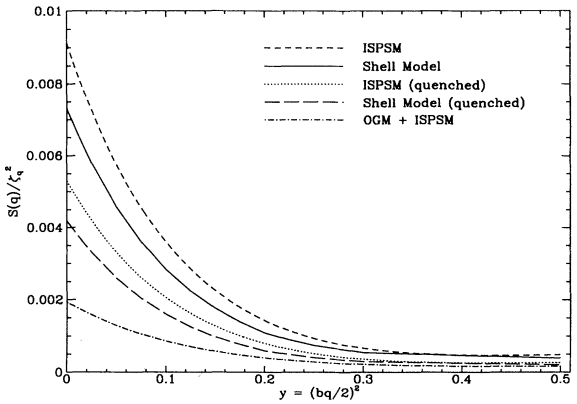

FIG. 9. Several different models of $S(q)$ for a pure $\tilde{B}$ scattering with ^{73}Ge: solid line=large space shell model result with no quenching [=solid line in Fig. 6(a)], long-dashed line=large space shell model result with isovector quenching [=solid line in Fig. 6(b)], short-dashed line=ISPSM result, dotted line=ISPSM result with isovector quenching, and the dot-dashed line=ISPSM result quenched to agree with the OGM at $q=0$.

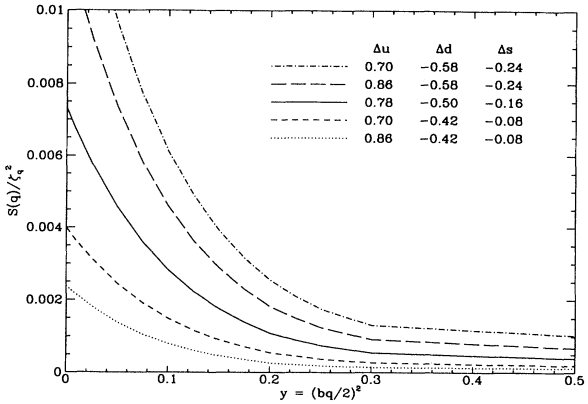

FIG. 10. $S(q)$ for a pure $\tilde{B}$, with EMC couplings, scattering with ^{73}Ge (large space calculation). Here we have varied the Δu, Δd, and Δs of the EMC result within the allowed errors (± 0.08) in deriving $a_{n(p)}$. The uncertainty due to the Δq's is currently much larger than the nuclear uncertainty; compare with Fig. 9.

case. Configuration mixing has made a major difference in this case because it has allowed for a large contribution to $\langle \mathbf{L}_p \rangle$, see Table III. The quenched IBFM result, when combined with a ISPSM response function, is in accord with the OGM+ISPSM result.

A final issue which bears mentioning, in both the zero and finite momentum transfer regimes, is the uncertainties in the nucleon coupling constants, a_n and a_p. So far, we have concentrated upon our attempts to improve the estimates of the cross section by generating more realistic nuclear wave functions. We have already demonstrated, in Figs. 5 and 6, the large differences in the matrix element which result from the EMC vs the NQM estimates of the proton's spin content. Here we wish to point out that even within the context of the EMC result, large differences in the rate are allowed. By varying the EMC values of the Δq's within the error bars we can vary $S(q)$ as shown in Fig. 10. Here the solid line is the same as the solid line in Fig. 9 and the other lines are obtained by varying Δu, Δd, and Δs within the allowed EMC errors. A huge range of values is allowed for $S(q)$. In fact, the uncertainty due to the Δq's is far larger than that arising due to nuclear processes. Hopefully, new experiments will eventually determine the Δq's with better precision. These new values, when coupled with the new picture of the nuclear structure presented here, will allow for a more accurate and complete description of $\tilde{\chi}N$ scattering for any neutralino.

In this section we have demonstrated that finite momentum transfers can have rather sizable effects on the $\tilde{\chi}N$ scattering cross section and hence on the scattering rate. In most cases, heavier $\tilde{\chi}$'s will have suppressed cross sections. This, coupled with the fact that it takes fewer heavy $\tilde{\chi}$'s than light ones to account for the dark matter, implies that it will be more difficult to detect neutralinos via the direct detection technique if they are very heavy.

V. DISCUSSION AND CONCLUSIONS

In this paper we have presented detailed nuclear shell model calculations of spin-dependent elastic $\tilde{\chi}N$ scattering from ^{29}Si and ^{73}Ge. Major $\tilde{\chi}$ dark matter detection programs based upon these two nuclei are well under way [15]. Our results reveal both the strengths and the weakness of previous, more phenomenological, analyses [7]. In both nuclei the ISPSM is found to be a poor approximation to the true nuclear configuration. In ^{29}Si at zero momentum transfer, the OGM finds results which are in accord with those of our calculations. This shows that, for this nucleus, the OGM adequately represents the configuration mixing. This is not the case in ^{73}Ge. In this nucleus, the shell model result is in severe disagreement with the OGM and quenched IBFM results. The main difference comes from the large amount of orbital angular momentum carried by the protons. This large value for $\langle \mathbf{L}_p \rangle$ violates a key assumption of the OGM and is not found in the IBFM. The larger value of $\langle \mathbf{L}_p \rangle$ in our calculation leads to a large improvement in the calculated vs measured magnetic moment of ^{73}Ge but still does not lead to complete agreement using free particle g factors. Thus we have discussed the difficult issue of quenching as it applies to ^{73}Ge. Even with quenching included our results still differ from those of the OGM and IBFM.

Unlike the OGM or the IBFM, it is straightforward to extend the shell model results to finite momentum transfer in a consistent manner. We find that finite momentum transfer will play an important role in determining the $\tilde{\chi}N$ scattering rate for very heavy neutralinos. Here again, we have compared the shell model results against the OGM combined with the ISPSM form factor. This latter approach seems to work well for ^{29}Si but significant disagreement is found for ^{73}Ge.

The major concern regarding our results is the validity of the ground-state wave functions we have generated. To help allay that concern, we have used our wave func-

tions to calculate a number of nuclear observables and compared the results to the measured values. In ^{29}Si excellent agreement was found for the magnetic moment, the excited state energy spectrum, and the first 3 spectroscopic factors. This was not surprising since we were able to use a well tested interaction in a well-defined model space. These calculations in ^{29}Si serve another useful purpose. The disagreement between the calculations and measurements in ^{29}Si serve to calibrate how accurately one can calculate nuclear properties in the shell model. Thus, the magnitude of the "errors" in the good calculation of silicon will help to establish how believable our calculation of ^{73}Ge is.

In ^{73}Ge the picture is more complicated. No phenomenological interaction has been developed for this region of the periodic table and fairly severe truncations to the model space have to be imposed to obtain manageable dimensions. Despite these obstacles, our best calculated ground state wave function for ^{73}Ge seems to be a good match when compared to experiment. We have obtained good agreement with the low-lying excited state energy spectrum. The ground state to ground state spectroscopic factor is also in fair agreement with experiment. The spectroscopic factors for transitions to excited states reveal that our model space does not contain enough configurations to completely describe the excited states, although the agreement between theory and experiment is not unreasonable. We reiterate that our model space was designed to describe the ground state and for that it does an acceptable job.

The final comparison is between magnetic moments. Using the large space wave function a significant improvement over the ISPSM or IBFM estimates of μ is found. Unfortunately, perfect agreement with experiment is not obtained but this is not expected or particularly damaging. Some sort of quenching of both μ and the GT spin matrix elements is almost universally required in shell model calculations of heavy nuclei. We find that an isovector spin quenching factor of 0.833 results in agreement with the measured value of the magnetic moment. This method and amount of quenching are consistent with previous studies of both GT and μ quenching and is therefore well motivated and simple. It is not manifestly obvious that quenching is needed in ^{73}Ge-$\tilde{\chi}$ scattering but, if so, we are confident that the correct answer lies in the range between the quenched and unquenched values of our calculation. In light of the above comparisons we feel that we have obtained an adequate description of the ground state structure of ^{73}Ge and that any calculation in a larger model space or with a different interaction will confirm our results. The disagreement between calculation and measurement in each case is somewhat larger than for ^{29}Si but is not so large as to cause us to doubt the result. The case is not airtight but 3 different lines of argument all indicate that the large space wave function is a better representation of the real nucleus than has previously been available.

As a summary and "users guide" we have collected the formulas, references, and suggested quenching methods in the appendix. Formulas for the spin-dependent neutralino cross section and the event detection rate in a bolometric detector are also given there.

In Sec. IV we describe the formalism for $\tilde{\chi}N$ scattering at finite momentum transfer. The cross section is given by Eq. (7) and all of the nuclear physics is contained in the spin structure function, $S(q)$, given by Eqs. (8)–(10). $S(q)$ may be decomposed into a pure isovector piece S_{11}, a pure isoscalar piece S_{00}, and an interference term S_{01}, see Eq. (10) (we will refer to these as S_{ij} where $i,j=0,1$). By taking suitable linear combinations of a_n and a_p, the isoscalar and isovector nucleon-$\tilde{\chi}$ coupling constants, a_0 and a_1, can be found for any composition neutralino. In Figs. 3 and 4 we presented the S_{ij} for ^{29}Si and ^{73}Ge, respectively. Along with a_0 and a_1 these plots can be used to compute the terms $a_i a_j S_{ij}$ which go into Eq. (10) to find $S(q)$ for any given $\tilde{\chi}$. As an alternative to this we have provided convenient fits to $S(q)$ for both nuclei in Eq. (11). These fits are quite accurate, for most $\tilde{\chi}$ compositions, in the regime $y \lesssim 0.15$. As noted in Sec. IV, there are certain combinations of a_0 and a_1 for which Eq. (11) is a poor approximation. With these words as a guide and using the formulas in the appendix, it should be straightforward to incorporate this work into calculations of the $\tilde{\chi}N$ scattering rate.

To help place this work in a larger context, we close by briefly discussing one final issue. This is a brief comparison of the spin dependent vs the spin-independent scattering. In addition to the spin-dependent scattering discussed at length in this paper, there is spin independent scattering which may produce competitive or larger scattering rates [4,7]. The spin independent piece is coherent, and thus, the cross section scales as (atomic number)^2. So, for heavy nuclei or light Higgs bosons this piece may dominate depending upon the mass and composition of the neutralino. Engel [7,18] has shown that the spin-independent form factor, corresponding to $S(q)$, falls off much faster at large q than does $S(q)$ itself. Thus, for very large $m_{\tilde{\chi}}$ spin dependent scattering is likely to dominate. Furthermore, for the pure $\tilde{\chi}$ states (e.g., a pure $\tilde{B}$), the coherent piece is suppressed (note, however, that recent work by Nojiri and Drees [38] may change this conclusion). Therefore spin-dependent scattering will probably dominate for these pure states. Outside of these two regimes it is not clear which piece, spin dependent or independent, will dominate the cross section and hence the rate.

ACKNOWLEDGMENTS

M.T.R. would like to thank his wife, Lisa, for assisting in a number of the computations. We would also like to thank J. Engel for several useful discussions. Work at LLNL was performed under the auspices of the U.S. Department of Energy under Contract No. W-7405-ENG-48 and DOE Nuclear Theory Grant SF-ENG-48. K.G. acknowledges support from a DOE Outstanding Junior Investigator grant.

APPENDIX: USERS GUIDE

In this appendix we collect the formulas necessary to convert our results for the nuclear matrix elements into

usable cross sections and interaction rates for dark matter detectors. We give *only* the spin-dependent cross section. To get the total cross section the spin-independent cross section [4,5,39,38] must be added to the cross sections below. We follow the notation and conventions of Refs. [4,5] with only slight modifications. In the limit of zero momentum transfer the cross section for spin-dependent elastic $\tilde{\chi}N$ scattering is

$$\sigma_{\rm SD}=\frac{24m_{\tilde{\chi}}^2 m_N^2 G_F^2}{\pi(m_{\tilde{\chi}}+m_N)^2}\frac{4}{3}\Lambda^2 J(J+1)\ , \tag{A1}$$

where m_N is the nuclear mass, $m_{\tilde{\chi}}$ is the neutrino mass, J is the total nuclear spin, G_F is the Fermi constant, and

$$\Lambda=\frac{\langle N|a_p\mathbf{S}_p+a_n\mathbf{S}_n|N\rangle}{J}=\frac{a_p\langle\mathbf{S}_p\rangle}{J}+\frac{a_n\langle\mathbf{S}_n\rangle}{J}\ . \tag{A2}$$

The spin averages $\langle\mathbf{S}_p\rangle$ and $\langle\mathbf{S}_n\rangle$ are given in Table III (but see below concerning quenching before using them), while a_p and a_n contain the details of the supersymmetric model, as well as the quark spin content of the proton and neutron:

$$a_{p(n)}=\sum_{u,d,s}A_q'\Delta q\ , \tag{A3}$$

$$A_q'=\frac{1}{2}T_{3L}^q(Z_3^2-Z_4^2)-x_q^2\left\{\frac{2m_q^2d_q^2}{4m_W^2}+[T_{3L}^qZ_2-\tan\theta_W(T_{3L}^q-e_q)Z_1]^2+\tan^2\theta_We_q^2Z_1^2\right\}\ , \tag{A4}$$

and

$$x_q^2=\frac{m_W^2}{m_{\tilde{q}}^2-m_{\tilde{\chi}}^2}\ . \tag{A5}$$

The various quantities used in the definition of A_q' involve the neutralino couplings and mass matrix, and can be found in Ref. [4]. For the special cases of photinos and B-inos, the $a_{p(n)}$ are given in Eqs. (12) and (13). The values Δq of the spin content of the nucleons are not well known. Some commonly used values are given in the text just after Eq. (12). The Δq for the neutron can be found from the Δq for the proton by switching Δu and Δd. (We note, for completeness, that new data on the deuteron's spin structure function has very recently become available. A new analysis incorporating this data along with the EMC results yields values of $\Delta u=0.80$, $\Delta d=-0.46$, and $\Delta s=-0.13$; all with an uncertainty of ±0.04 [40].)

For ^{29}Si, we suggest using the values of $\langle\mathbf{S}_n\rangle$ and $\langle\mathbf{S}_p\rangle$ from the "shell model" row of Table III with no quenching. For ^{73}Ge we advocate quenching the isovector piece of the nucleon-$\tilde{\chi}$ coupling constants a_p and a_n. Hence one should not use Eq. (2). To quench the isovector piece of a_p and a_n one first computes a_p and a_n from Eq. (A3) and then constructs the isovector and isoscalar coupling constants: $a_1=a_p-a_n$ and $a_0=a_p+a_n$. The isovector piece is then multiplied by the quenching factor, $a_1'=0.833a_1$. In the zero momentum transfer limit, the a_p and a_n are then recalculated using the quenched value a_1'. These values are then used in Eq. (A2) in place of those calculated directly from Eq. (A3). In other words to quench by a factor $Q=(0.833)$ in Eq. A(2) make the replacement

$$\begin{aligned}a_p\Longrightarrow a_p'&=\tfrac{1}{2}[a_p(1+Q)+a_n(1-Q)]\\&=0.917a_p+0.0835a_n\ ,\\ a_n\Longrightarrow a_n'&=\tfrac{1}{2}[a_n(1-Q)+a_n(1+Q)]\\&=0.0835a_p+0.917a_n\ .\end{aligned} \tag{A6}$$

In this scheme one uses the values of $\langle\mathbf{S}_n\rangle$ and $\langle\mathbf{S}_p\rangle$ from the "shell model (large)" row of Table III (not the "quenched" row).

To make contact with previous work, we note that the ISPSM (single particle shell model) can be obtained from Eq. (A1) by the simple substitution

$$\Lambda^2\Longrightarrow a_{p(n)}^2\lambda^2\ , \tag{A7}$$

where in the ISPSM only one of either a_n or a_p contributes and

$$\lambda=\frac{1}{2}\left[1+\frac{s_{p(n)}(s_{p(n)}+1)-l_{p(n)}(l_{p(n)}+1)}{J(J+1)}\right]=\frac{s_{p(n)}}{J}\ , \tag{A8}$$

where J is the total nuclear angular momentum ($J=s_{p(n)}+l_{p(n)}$), $s_{p(n)}$ and $l_{p(n)}$ are the unpaired proton or neutron spin and orbital angular momentum, respectively. For example, in the ISPSM, ^{73}Ge is modeled as a neutron with $l_n=4$ and $J=\frac{9}{2}$, while ^{29}Si is modeled as a neutron with $l_n=0$, and $J=\frac{1}{2}$.

When the neutralino mass is over a few tens of GeV, it becomes important to include the effect of finite momentum transfer. Eqs. (7)–(11) in the text show how to include this effect. To implement the suggested quenching scheme for ^{73}Ge simply make the replacement Eq. (A6) (or equivalent $a_1\rightarrow a_1'=0.833a_1$) in Eqs. (7)–(11). Note in particular that Eq. (9c) can be written

$$S(0)=\frac{2J+1}{\pi}\Lambda^2J(J+1)\ . \tag{A9}$$

Since we work in the z projection of the maximally stretched state, the function $f(N)$ introduced in Eq. (9c) has the form $f(N)=f(J)=(2J+1)(J+1)/J$.

The rate per unit detector mass with which neutralinos interact with a detector is given by [9,4,7]

$$R = \frac{\rho}{m_{\tilde{\chi}} m_N} \int v\, dv\, f(v) \int_0^{4M_r^2 v^2} dq^2 \frac{d\sigma}{dq^2} , \qquad \text{(A10)}$$

where m_N is the mass of the nucleus, $M_r = m_N m_X/(m_N + m_X)$, $d\sigma/dq^2$ is given in Eq. (7), $\rho \simeq 0.4$ GeV/cm^3 is the halo density (assumed to consist entirely of neutralino's), $f(v)$ is the velocity distribution of the halo, and $v_0 \simeq 220$ km s^{-1} is the circular velocity in the halo, which sets the scale for the halo gravitational potential. For simplicity one can choose a Maxwellian distribution of velocities $f(v) = 4v^2 \exp(-v^2/v_0^2)/(v_0^3\sqrt{\pi})$, or one can follow [9,4,41] and include the effects of the Sun and Earth motion, as well as the effect of a detector threshold.

Integrating Eq. (A10) one gets

$$R = \frac{2}{\sqrt{\pi}} \eta_c \eta_v \frac{\rho}{m_{\tilde{\chi}} m_N} v_0 \sigma_{\rm SD} , \qquad \text{(A11)}$$

where [9] $\eta_v \approx 1.3$ gives a correction for the speed of the Sun through the halo, and the effect of integrating over q^2 is summarized by

$$\eta_c = \sigma_{\rm SD}^{-1} \int dq^2 \frac{d\sigma}{dq^2} .$$

In the limit of zero momentum transfer, the q^2 integral in Eq. (A1) becomes $\sigma_{\rm SD}$ and $\eta_c \to 1$. Note again that to find the total event rate one must include the spin-independent piece of the cross section which is not considered in this paper.

In order to evaluate η_c one may use the fits to $S(q)$ given in Eq. (11). This will give an approximation which should be good for most neutralinos (but see the cautions in the text). We rewrite Eq. (11) as

$$S^{\rm fit}(y) = \sum_{i=1}^{3} A_i e^{-B_i y} ,$$

where the A_i and B_i are given in Eq. (11), and $y = (bq/2)^2$. For ^{73}Ge, $b \simeq 2.04$ fm, and for ^{29}Si, $b \simeq 1.75$ fm. Note now $\sum A_i = S^{\rm fit}(0)$. Then

$$\eta_c = \left\{ \sum_i A_i \frac{1-\beta_i}{\alpha_i \left[\frac{1}{2} + p^2 + \frac{p e^{-p^2}}{\sqrt{\pi}\,\mathrm{erf} p} \right]} \right\} \Big/ \sum_i A_i , \qquad \text{(A12)}$$

where

$$\beta_i = \frac{\exp\left[\frac{-p^2\alpha_i}{1+\alpha_i}\right] \mathrm{erf}\left[\frac{p}{\sqrt{1+\alpha_i}}\right]}{\sqrt{1+\alpha_i}\,\mathrm{erf}(p)} ,$$

$p = v_{\rm SUN}/v_0 \approx 1$, and $\alpha_i = B_i b^2 v_0^2 M_r^2$. In the limit $p = 0$ (the limit of a stationary Sun or isotropic velocity distribution),

$$\eta_c \to \sum_i A_i \alpha^{-1} [1 - 1/(1+\alpha_i)] \Big/ \sum_i A_i .$$

[1] V. Trimble, Annu. Rev. Astron. Astrophys. **25**, 425 (1989); J. R. Primack, B. Sadoulet, and D. Seckel, Annu. Rev. Nucl. Part. Sci. **38**, 751 (1988).

[2] M. S. Turner, Phys. Scr. **T36**, 167 (1991); J. Ellis, *ibid.* **T36**, 142 (1991).

[3] H. E. Haber and G. L. Kane, Phys. Rep. **117**, 75 (1985).

[4] K. Griest, Phys. Rev. D **38**, 2357 (1988).

[5] J. Silk, K. A. Olive, and M. Srednicki, Phys. Rev. Lett. **53**, 624 (1985); M. Kamionkowski, Phys. Rev. D **44**, 3021 (1991).

[6] M. W. Goodman and E. Witten, Phys. Rev. D **31**, 3059 (1985).

[7] J. Engel, S. Pittel, and P. Vogel, Int. J. Mod. Phys. E **1**, 1 (1992).

[8] J. Ashman *et al.*, Phys. Lett. B **206**, 364 (1988); J. Ashman *et al.*, Nucl. Phys. **B328**, 1 (1989).

[9] A. K. Drukier, K. Freese, and D. N. Spergel, Phys. Rev. D **33**, 3495 (1986); K. Freese, J. Freeman, and A. Gould *ibid.* **37**, 3388 (1988).

[10] J. Ellis and R. A. Flores, Nucl. Phys. **B307**, 883 (1988).

[11] J. Engel and P. Vogel, Phys. Rev. D **40**, 3132 (1989).

[12] J. Ellis and R. A. Flores, Phys. Lett. B **263**, 259 (1991).

[13] A. F. Pacheco and D. Strottman, Phys. Rev. D **40**, 2131 (1989).

[14] J. Engel *et al.*, Phys. Lett. B **275**, 119 (1992).

[15] B. A. Young *et al.*, Nucl. Instrum. Methods **A311**, 195 (1992); T. Shutt *et al.*, Phys. Rev. Lett. **69**, 3425 (1992); **69**, 3531 (1992); B. A. Young, in *Proceedings of the Third International Conference on Advanced Technology and Particle Physics,* edited by E. Borchi *et al.* (Elsevier, Amsterdam, 1993).

[16] D. A. Resler and S. M. Grimes, Comput. Phys. **2** (3), 65 (1988).

[17] F. Iachello, L. M. Krauss, and G. Maino, Phys. Lett. B **254**, 220 (1991).

[18] J. Engel, Phys. Lett. B **264**, 114 (1991).

[19] J. D. Walecka, in *Muon Physics,* edited by V. W. Hughes and C. S. Wu (Academic, New York, 1975), Vol. 2, p. 113; T. W. Donnelly and R. D. Peccei, Phys. Rep. **50**, 1 (1979); T. W. Donnelly and W. C. Haxton, At. Data Nucl. Data Tables **23**, 103 (1979).

[20] B. H. Wildenthal, in *Progress in Particle and Nuclear Physics,* edited by D. H. Wilkinson (Pergamon, Oxford, England, 1984), Vol. 11, p. 5.

[21] B. A. Brown, in *Nuclear Physics in the 1990's,* edited by D. H. Feng *et al.* [Nucl. Phys. **A522**, 221c (1991)].

[22] C. M. Lederer and V. S. Shirley, *Table of Isotopes,* 7th ed. (Wiley, New York, 1978).

[23] K. L. G. Heyde, *The Nuclear Shell Model* (Springer-Verlag, Berlin, 1990), p. 226; P. J. Brussard and P. W. M. Glaudemans, *Shell-Model Applications in Nuclear Spectroscopy* (North-Holland, Amsterdam, 1977), p. 144.

[24] P. M. Endt, Nucl. Phys. **A521**, 1 (1990).

[25] G. J. Mathews *et al.*, Phys. Rev. C **32**, 796 (1985).

[26] F. Petrovich, H. McManus, V. A. Madsen, and J. Atkinson, Phys. Rev. Lett. **22**, 895 (1969).

[27] A. Kallio and K. Kolltviet, Nucl. Phys. **53**, 87 (1964).
[28] B. A. Brown and B. H. Wildenthal, Nucl. Phys. **A474**, 290 (1987).
[29] W. A. Richter *et al.*, Nucl. Phys. **A523**, 325 (1991).
[30] W. A. Yoh, S. E. Darden, and S. Sen, Nucl. Phys. **A263**, 419 (1976).
[31] B. A. Brown and B. H. Wildenthal, At. Data Nucl. Data Tables **33**, 347 (1985).
[32] J. Ellis *et al.*, Nucl. Phys. **B238**, 453 (1984).
[33] K. Griest and L. Roszkowski, Phys. Rev. D **46**, 3309 (1992).
[34] K. Griest, M. Kamionkowski, and M. S. Turner, Phys. Rev. D **41**, 3565 (1990); K. A. Olive and M. Srednicki, Nucl. Phys. **B355**, 208 (1991).
[35] L. Roszkowski, University of Michigan Report No. UM-TH-9306 (unpublished).
[36] R. L. Jaffe and A. Manohar, Nucl. Phys. **B337**, 509 (1990).
[37] R. Flores, K. A. Olive, and M. Srednicki, Phys. Lett. B **237**, 72 (1990).
[38] M. Drees and M. M. Nojiri, Phys. Rev. D **47**, 4226 (1993).
[39] R. Barbieri, M. Frigeni, and G. G. Guidice, Nucl. Phys. **B313**, 725 (1989).
[40] J. Ellis and M. Karliner, Phys. Lett. B **313**, 131 (1993).
[41] K. Griest, Phys. Rev. D **37**, 2703 (1988).